

Hyperfine structure of ND₃

Jacqueline van Veldhoven,^{1,2} Rienk T. Jongma,^{1,2} Boris Sartakov,³ Waldo A. Bongers,¹ and Gerard Meijer^{1,2}

¹*FOM-Institute for Plasmaphysics Rijnhuizen, P.O. Box 1207, NL-3430 BE Nieuwegein, The Netherlands*

²*Department of Molecular and Laser Physics, University of Nijmegen, Toernooiveld 1, NL-6525 ED Nijmegen, The Netherlands*

³*General Physics Institute RAS, Vavilov Street 38, 119991 Moscow, Russia*

(Received 17 April 2002; published 23 September 2002)

Pure inversion spectra for the $|J,K\rangle=|1,1\rangle$ level of ¹⁴ND₃ and of ¹⁵ND₃ are recorded at 10 kHz resolution using a molecular-beam microwave-UV double-resonance spectrometer. The observed spectra are fully assigned, and the energies of all $|J,K\rangle=|1,1\rangle$ hyperfine levels of both deuterated ammonia isotopomers are obtained. The shifting and splitting of the manifold of hyperfine levels in external electric fields is calculated and its implications for molecular-beam deceleration and trapping experiments are discussed.

DOI: 10.1103/PhysRevA.66.032501

PACS number(s): 33.20.Bx, 33.55.Be, 33.80.Ps

I. INTRODUCTION

There currently is a rapidly growing interest in the physics of cold molecules, in general [1,2], and in the physics of cold polar gases, in particular [3]. This interest stems, for instance, from the anticipated importance of the anisotropic interaction between electric dipoles on the formation of a molecular Bose-Einstein condensate [4], from the possibility to use single-component cold polar gases for the observation of the superfluid transition [5], and from the possibility to use arrays of trapped polar molecules for quantum computation [6].

There are now three techniques via which samples of trapped cold molecules have been produced. Photoassociation of trapped alkali atoms has been used to produce translationally cold alkali dimers, which have subsequently been trapped in a far-off-resonance optical trap [7] and, more recently, in a quadrupole magnetic trap [8]. Magnetic trapping of paramagnetic molecules thermalized in a He buffer gas has been demonstrated as well [9]. In the third method, explored in our laboratory, time-varying electric fields are used to first decelerate pulsed beams of polar molecules [10–12], after which “bunches” of these slow molecules are electrostatically confined [13,14]. In the most recent experiments, it is demonstrated that in a single deceleration and loading cycle, both (bosonic) ¹⁴ND₃ and (fermionic) ¹⁵ND₃ ammonia isotopomers can be trapped, even simultaneously, at densities higher than 10⁷/cm³ and at temperatures of around 25 mK [15].

To further increase the phase-space density, i.e., to further increase the number density and/or to decrease the temperature, evaporative cooling [16] of the electrostatically trapped ammonia molecules will be experimentally investigated. In such experiments, selective removal of the hottest ammonia molecules can be achieved when an rf knife is used to induce transitions from the trapped to the untrapped component of the $|J,K\rangle=|1,1\rangle$ inversion doublet. For this, the hyperfine structure of these particular levels in ammonia, with and without electric fields, needs to be accurately known. Knowledge on the hyperfine structure of ammonia is also required to prepare these molecules in selected (subsets of) hyperfine levels in either one of the components of the inversion doublet prior to scattering or trapping experiments.

In this paper we report on the pure inversion spectra for the $|J,K\rangle=|1,1\rangle$ level of ¹⁴ND₃ and ¹⁵ND₃. Although the hyperfine structure of ¹⁴NH₃ has been studied in the utmost detail [17–25] and its inversion doubling is often being used as a textbook example, the inversion spectra of the deuterated isotopomers of ammonia have received considerably less attention [26–32]. Surprisingly, to the best of our knowledge, the hyperfine structure for the deuterated isotopomers has neither been resolved nor analyzed at all so far. In the experiments reported here, the inversion spectra in the (1.4–1.6)-GHz region are recorded at 10 kHz resolution using a molecular-beam microwave-UV double-resonance spectrometer. The observed spectra are quantitatively understood, and the energies of all $|J,K\rangle=|1,1\rangle$ hyperfine levels of both deuterated ammonia isotopomers are obtained. Implications of the behavior of the manifold of hyperfine levels in electric fields, both for deceleration and for trapping experiments, are discussed.

II. EXPERIMENT

The experiments are performed in a pulsed molecular-beam spectrometer, schematically shown in Fig. 1. A pulsed valve (modified General Valve, Series 9) expands a 150- μ s-duration gas pulse containing typically 5% of ¹⁴ND₃ or ¹⁵ND₃ seeded in Xe into the source chamber. The most intense part of the beam, which has a mean velocity of around 365 m/s, enters the second vacuum chamber via a skimmer with a 1.5-mm-diameter opening. Both vacuum chambers are pumped by 500 l/s turbo molecular pumps. In the second chamber, the beam passes through a 15-cm-long hexapole state selector, the entrance of which is mounted 15.8 cm downstream from the nozzle. The hexapole consists of 4-mm-diameter electrodes, positioned on the outside of a circle with a 4 mm radius. In the molecular beam, about 60% of all the ND₃ molecules will reside in the $|J,K\rangle=|1,1\rangle$ inversion doublet, as this is the ground state for para-ammonia molecules. In the hexapole, molecules in quantum states with a positive Stark effect (the upper component of the inversion doublet; *a* symmetry) are focused, whereas molecules in quantum states with a negative Stark effect (the lower component of the inversion doublet; *s* symmetry) are defocused. This results, therefore, in population inversion between many

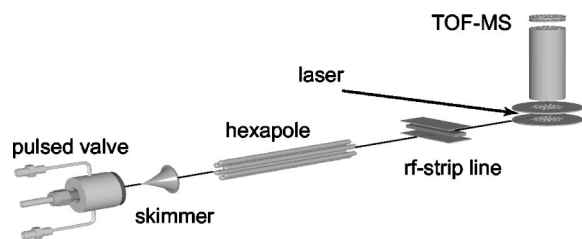


FIG. 1. Scheme of the pulsed molecular-beam spectrometer. ND_3 seeded in Xe is expanded from a pulsed valve. After passage through the skimmer, the ammonia molecules fly through a (pulsed) hexapole lens which focuses (defocuses) the molecules that are in the upper (lower) component of the inversion doublet. Population inversion between these components therefore exists when the molecules enter the ≈ 3 -cm-long rf-interaction region behind the hexapole. There, radiation is applied that is resonant with the $|J, K\rangle = |1, 1\rangle_a \rightarrow s$ transition. By selectively probing the population in the s component of the inversion doublet via UV laser ionization as a function of the rf frequency, the pure inversion spectrum is recorded (almost) background-free.

hyperfine levels of the two inversion doublet components close to the molecular-beam axis, downstream from the hexapole.

At a distance of 21 cm from the end of the hexapole, the molecular beam passes through an rf stripline. There, rf radiation that is resonant with transitions between hyperfine levels in the upper and lower component of the inversion doublet can be applied to the molecules. For $^{14}\text{ND}_3$, radiation around 1.6 GHz is required [32], while the corresponding transition for $^{15}\text{ND}_3$ is around 1.4 GHz [31]. The stripline is impedance matched [33] to the rf source (50 Ω) and is built out of three aluminum electrodes. The outer two electrodes, both at ground potential, have a width of 40 mm. These electrodes are separated by 19 mm. The middle electrode, connected to the rf source, is 20 mm wide and 3 mm thick. With this geometry, the reflected power is below 1% over the entire frequency range used in the experiments, while the transmitted power is typically 85%. The molecular beam passes along the center of the 8-mm opening between the lower two electrodes. The field that the molecules experience is fairly homogeneous over the 20 mm width of the middle electrode, and gradually decreases on either side over a typical distance of 5 mm. An rf synthesizer (Hewlett Packard, HP8657B), providing radiation throughout the 0.1–2060 MHz range with a maximum output power of 50 mW, is used as radiation source. Both the frequency and the output power of the rf source can be computer controlled. Calibration of the frequency of the radiation of the rf source to about 10^{-8} is achieved by connecting the output to a frequency counter, stabilized by an atomic-clock reference signal.

The hexapole is set such that the molecular beam is focused in the laser detection region, some 15 cm downstream from the rf-interaction region. There, the molecules are ionized via a (2+1)-resonance enhanced multiphoton ionization process [34]. The required laser radiation of around 317 nm is obtained by frequency doubling the output of a Nd:YAG (yttrium aluminum garnet) laser pumped pulsed dye-laser system (Spectra Physics, GCR-190/Radiant, Narrowscan

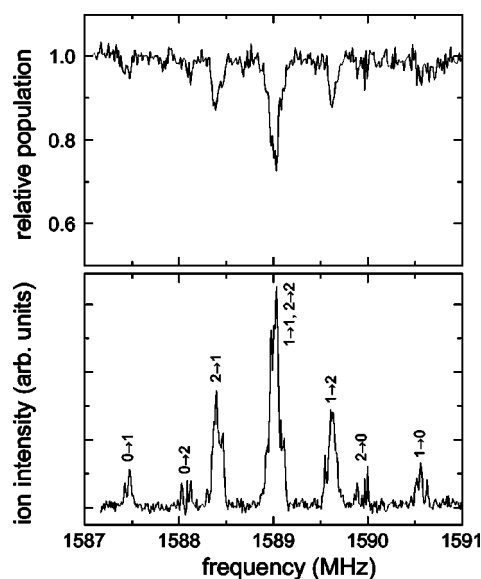


FIG. 2. Pure inversion spectrum of $^{14}\text{ND}_3$ ($|J, K\rangle = |1, 1\rangle$), measured by probing both the upper component (upper trace) and the lower component (lower trace) of the inversion doublet. The spectra are recorded at high microwave powers (1 mW) and are power broadened. Assignment of the main $F'_1 \rightarrow F''_1$ features is given in the spectrum.

combination). Typically, about 10 mJ/pulse in a 0.05 cm^{-1} spectral bandwidth is focused into the detection region by a lens with a focal length of 50 cm, intersecting the molecular beam at right angles. The ions produced in the focus of the laser are extracted into a short time-of-flight mass spectrometer and are mass-selectively detected.

In the laser detection region, the density of ammonia molecules in either the a -symmetry or the s -symmetry component can be probed. Microwave spectra are obtained by scanning the rf frequency while keeping the detection laser fixed on a resonance. When the a level is probed (on the $\Delta K = +1$, $\Delta J = +2$ transition at $31\,511.0 \text{ cm}^{-1}$ for $^{14}\text{ND}_3$ [34], and redshifted over some 10 cm^{-1} for $^{15}\text{ND}_3$), a microwave transition is observed as a decrease in the ion signal, whereas an increase in the ion signal is observed when the s level is probed (on the $\Delta K = +1$, $\Delta J = +2$ transition at $31\,136.7 \text{ cm}^{-1}$ for $^{14}\text{ND}_3$ [34], and again somewhat redshifted for $^{15}\text{ND}_3$). The best signal-to-noise ratio for the inversion spectra is obtained in the latter situation, as rf transitions are then measured as an increase in the ion signal against a strongly reduced background signal. The remaining background signal is due to ammonia molecules originally already residing in the lower component of the inversion doublet that travel close to the hexapole axis and that are hardly deflected. The insertion of a 1-mm-diameter beam stop directly behind the hexapole reduces this background signal to about 70% of its original value and thereby further increases the detection sensitivity.

To focus ammonia molecules in low-field seeking states in the laser detection region, a constant voltage difference of about 2.5 kV can be applied to neighboring rods of the hexapole. As the electric field near the entrance and the exit of the hexapole drops off to zero on a typical distance of about 5

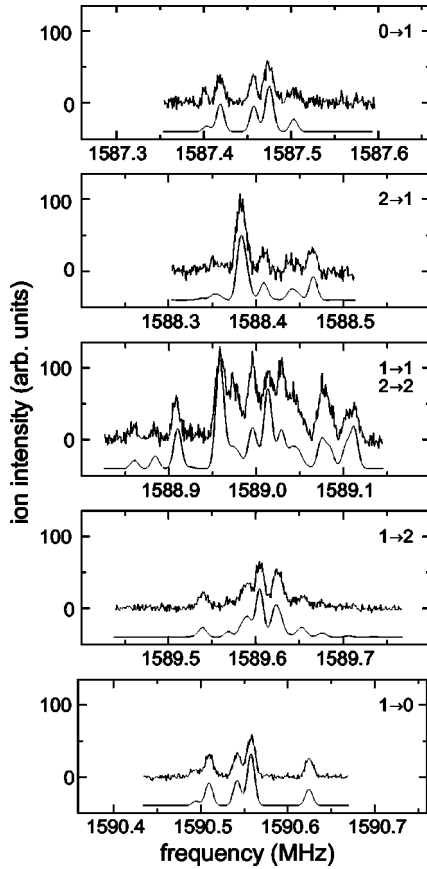


FIG. 3. The five main $F'_1 \rightarrow F''_1$ transitions in the microwave spectrum of $^{14}\text{ND}_3$, recorded with a spectral resolution of 10 kHz. The upper trace in each of the graphs shows the experimental spectrum while the lower trace is the simulated spectrum, using the parameters in the Hamiltonian as obtained from the best fit.

mm, the molecules then experience an increasing and decreasing electric field on the tens of microseconds time scale. This is slow enough for the molecules to follow the Stark curves adiabatically. This results, however, in a complicated population distribution over the various hyperfine levels for those molecules that enter the rf-interaction region; hyperfine levels composed of (at least some) M_F sublevels that are low-field seeking will be predominantly populated. Molecules in some hyperfine levels will not be focused at all, in which case microwave transitions originating from these levels are absent in the spectra, complicating the spectral assignment. Therefore, in most of the experiments reported below, a 8.5 kV voltage difference that can be rapidly switched on and off is applied to neighboring hexapole rods for a 110 μs duration when the gas pulse is completely inside the hexapole. The high voltage is switched on and off on a 200 ns time scale, which is sufficiently fast to break the adiabatic following as the hyperfine levels are all within a few megahertz from each other (*vide infra*). This leads to a redistribution of the population over various hyperfine levels within a component of the inversion doublet, obeying the $\Delta M_F = 0$ selection rule. As the switching off of the electric field does not affect the velocity of the molecules, molecules residing in hyperfine levels of the upper inversion doublet component

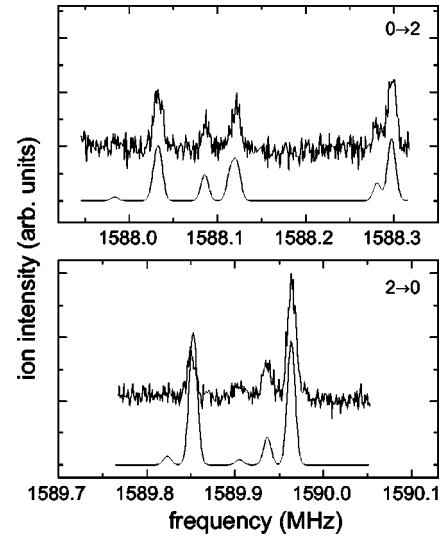


FIG. 4. The weak $F'_1 = 0 \rightarrow F''_1 = 2$ and $F'_1 = 2 \rightarrow F''_1 = 0$ transitions for $^{14}\text{ND}_3$, recorded at increased rf powers of 0.25 mW and 0.13 mW, respectively. Underneath the experimental spectra, the simulated spectra are shown.

which almost experience no Stark effect, will now be focused in the detection region as well. In the simulation of the spectra it is assumed that upon entering the rf-transition region, all hyperfine levels of the upper inversion doublet component are equally populated, which appears to describe the experimental situation rather well.

III. RESULTS AND DISCUSSION

A. Inversion spectra of $^{14}\text{ND}_3$

In Fig. 2 an overview spectrum is shown of the $|J, K\rangle = |1, 1\rangle$ inversion spectrum of $^{14}\text{ND}_3$ as obtained by probing the population in the upper component (top trace) and in the lower component (bottom trace) of the inversion doublet under otherwise identical conditions. It is clear that the lower spectrum has the better signal-to-noise ratio. To be able to also observe the weaker spectral features, a relatively high rf power of 1 mW is used for these measurements. Under these conditions many of the transitions observed in the spectrum are saturated and the observed linewidth for those transitions is mainly determined by power broadening. From the measurements presented in the upper trace it is seen that up to 30% of the molecules originally distributed over hyperfine levels of the a -symmetry component are optically pumped to a selected subset of hyperfine levels in the s -symmetry component.

The main structure observed in these spectra can be understood by only taking the quadrupole interaction of the ^{14}N nucleus into account. This is the dominant interaction term, and leads to a splitting of each component of the inversion doublet into three (groups of) levels. Each of these (groups of) levels can be labeled by the quantum number F_1 , where $\vec{F}_1 = \vec{J} + \vec{I}_N$, \vec{I}_N being the nitrogen nuclear-spin vector. The $F'_1 \rightarrow F''_1$ assignment of the main groups of lines is indicated in the lower spectrum of Fig. 2. It should be noted that the

TABLE I. Adjustable parameters in the Hamiltonian, together with their correspondence to parameters in the more commonly used notation. Their values as obtained from the best fit to the experimentally observed $^{14}\text{ND}_3$ and $^{15}\text{ND}_3$ transition frequencies are given. The standard deviation of the fit is about 2 kHz, both for $^{14}\text{ND}_3$ and $^{15}\text{ND}_3$.

Symmetry group formalism	Ref. [25]	Parameters (MHz) for			
		$^{14}\text{NH}_3$ ^a	$^{15}\text{NH}_3$ ^b	$^{14}\text{ND}_3$	$^{15}\text{ND}_3$
c_t ^c	Ω_t	23694.4955	22613.4955	1589.0094(3)	1430.3384(6)
c_{QN}	$\sqrt{15/8}eQq_s$	-5.6025	0	-5.591(2)	0
δc_{QN}	$\sqrt{15/8}(eQq_a - eQq_s)$	0.0038	0	0.0000	0
c_{JN1}	$-(2a+b)/\sqrt{3}$	-0.0117	0.0165	-0.0062(4)	0.0082
c_{JN2}	$-\sqrt{10/3}(a-b)$	-0.0002	0.0003	-0.00018	0.00013
c_{JD1}	$-(3A+C)$	0.0549	0.0549	0.005(1)	0.004(1)
c_{JD2}	$\sqrt{10}C$	-0.0030	-0.0030	-0.0002	-0.0002
c_{JD3}	$\sqrt{30}B$	0.0802	0.0802	0.0062	0.0062
c_{ND1} ^d	$-3\sqrt{10}D_1$	0.0231	-0.0323	0.0035	-0.0050
c_{ND2} ^d	$\sqrt{30}D_2$	-0.0575	0.0806	-0.009(2)	0.017(6)
c_{DD1} ^d	$3\sqrt{5/2}D_3$	0.1289	0.1289	0.003	0.003
c_{DD2} ^d		0.2233	0.2233	0.005	0.005
c_{QD1}		0	0	-0.221(9)	-0.221(8)
c_{QD2}		0	0	0.429(3)	0.434(3)

^aValues taken from Ref. [25].

^bValues scaled to parameters from $^{14}\text{NH}_3$.

^cOnly the statistical error is indicated. Electric-field components along the molecular-beam axis can cause a maximum Doppler shift of 1.8 kHz. As the field is directed mainly perpendicular to the molecular-beam axis, this effect will be small, however.

^dInitial approximate values for these parameters can be calculated from the geometry ($R_{\text{ND}} \approx 1.02 \text{ \AA}$ and $\beta \approx 68^\circ 53'$) of the molecule via the following formulas: $c_{ND1} \approx 3\sqrt{10}(g_N/I_N)(g_D/I_D)\mu_0^2[(3/2)\sin^2\beta - 1]/R_{\text{ND}}^3$, $c_{ND2} \approx -3\sqrt{15/2}(g_N/I_N)(g_D/I_D)\mu_0^2 \sin^2\beta/R_{\text{ND}}^3$, $c_{DD1} \approx 3\sqrt{5/2}[(g_D/I_D)\mu_0]^2/R_{\text{DD}}^3$, $c_{DD2} \approx \sqrt{3}c_{DD1}$, in which μ_0 is the nuclear magneton. In the fitting procedure only the largest parameter (c_{ND2}) could be further refined.

$0 \rightarrow 1$ and $0 \rightarrow 2$ transitions, as well as some other lines originating from $F'_1 = 0$ levels, are only observed when the hexapole is rapidly switched off, as is done here, i.e., when redistribution of the population over the hyperfine levels occurs. As F_1 is almost a good quantum number, the $\Delta F_1 = \pm 2$ transitions are only weakly allowed, and are therefore considerably less power broadened.

In Fig. 3 experimental high-resolution inversion spectra of the spectral regions around the five strongest $F'_1 \rightarrow F''_1$ transitions are shown. All five spectra are plotted on the same intensity scale, and are recorded under identical conditions. For these measurements the rf power is reduced to $5 \mu\text{W}$ to stay sufficiently far away from saturation. For all $F'_1 \rightarrow F''_1$ transitions, a rich substructure is observed. The width of isolated spectral lines is observed to be about 10 kHz, in good agreement with the linewidth expected for transit-time broadening of the (relatively slow) molecules passing through the effectively 30-mm-wide rf-interaction region. The lower trace in each of the graphs is a simulation based on the best fit to the experimentally determined transition frequencies, as will be discussed in more detail below. In the simulation, a Gaussian line shape with a 10-kHz linewidth (full width at half maximum) is used. Both the peak position

and the relative intensities of most features are well reproduced.

In Fig. 4 the corresponding high-resolution spectra for the weaker $\Delta F_1 = \pm 2$ transitions, recorded with higher rf powers, are shown. These spectra are also well reproduced by simulations based on the results of the best fit, shown as the lower trace in each graph.

It should be emphasized that for all high-resolution microwave spectra presented here, no significant changes are observed when the ionization laser is tuned to a different transition, i.e., when a different intermediate state is used to probe the population in the same component of the inversion doublet; apparently there is no significant hyperfine-level selectivity in the UV-laser based detection process.

B. Energy levels, fitting parameters, and Stark effect for $^{14}\text{ND}_3$

To assign and simulate the experimental spectra, a general formalism to describe the Hamiltonian for the four different symmetric top ammonia isotopomers ($^{14}\text{NH}_3$, $^{15}\text{NH}_3$, $^{14}\text{ND}_3$, and $^{15}\text{ND}_3$) is used. The generalized tensor coupling scheme that is set up allows the Hamiltonian to be tested on

the experimentally well-characterized ¹⁴NH₃ system [25], prior to being applied to the more complex deuterated ammonia isotopomers.

To describe the hyperfine structure in the required detail, all the spin-spin and spin-rotation terms off-diagonal in F_1 need to be taken into account [25]. As the three deuterium atoms are in equivalent positions, their nuclear spins are coupled to give the overall deuterium nuclear-spin angular-momentum vector \vec{I}_D . This vector couples to \vec{F}_1 to obtain \vec{F} , providing the (only) good quantum numbers F and M_F . Note that, as the formalism is generalized to describe all isotopomers mentioned above, any time that deuterium is mentioned, one can read hydrogen instead as well. The total wave function of the molecule is represented via the coupling of vibration (inversion tunneling), rotation, and spin wave functions, all of them being treated as tensors. Both the wave functions and the Hamiltonian are reduced to the irreducible symmetry representation. A detailed description of this formalism will be given elsewhere [35].

The parameters used in the Hamiltonian are given in the first column of Table I. Here we will just briefly indicate the physical meaning of the various parameters, in order of their appearance in the table. The parameter c_t describes the magnitude of the inversion splitting. The parameter c_{QN} represents the strength of the quadrupole interaction of the nitrogen atom, while δc_{QN} is a correction to that term for the upper inversion doublet component only, probably due to a slight difference in the internal electric field [25]. The parameters c_{JN1} and c_{JN2} determine the coupling strength of the rotational angular momentum \vec{J} and the nuclear spin of the nitrogen atom \vec{I}_N . The next three parameters, c_{JD1} , c_{JD2} , and c_{JD3} describe the interaction of the rotational angular momentum with the total nuclear spin of the deuterium atoms. The parameters c_{ND1} and c_{ND2} describe the spin-spin interaction between the nitrogen and deuterium atoms, while c_{DD1} and c_{DD2} describe the spin-spin interaction between two deuterium atoms. Finally, c_{QD1} and c_{QD2} describe the quadrupole interaction of the deuterium atoms. The corresponding parameters in the more conventional representation of the Hamiltonian [18,25] are given in Table I as well.

An approximate initial value for most parameters in the Hamiltonian for ¹⁴ND₃ is obtained by an appropriate scaling of the corresponding (known) parameters for ¹⁴NH₃, given in the third column of Table I. To do so, the formula for the nuclear magnetic moment as given in Ref. [36] is used. It is noted that the nuclear magnetic moment has to be scaled to the absolute value of the nuclear spin, which is actually not done in most textbooks and which is the (trivial) explanation for the apparent discrepancy discussed at length in the paper of Kukulich [37]. The parameters in the Hamiltonian that best describe the experimental data for ¹⁴ND₃, as obtained by fitting the observed transition frequencies of 33 more or less isolated lines, are listed in the fifth column of Table I. For each parameter the standard deviation from the fit is indicated between brackets. Those parameters that are listed without standard deviation are kept fixed in the fitting procedure at the values obtained from direct scaling from ¹⁴NH₃, as these parameters cannot be further refined, i.e., as

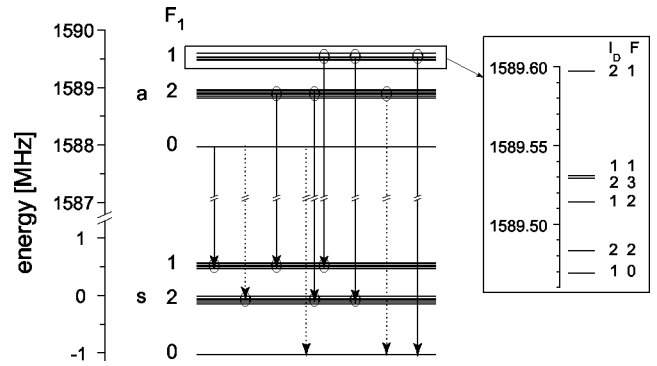


FIG. 5. Energy-level structure of ¹⁴ND₃ ($|J,K\rangle=|1,1\rangle$). The quadrupole interaction of the ¹⁴N atom causes the main splitting of both the upper and the lower component of the inversion doublet in three levels, labeled with the quantum number F_1 . The nuclear spins of the deuterium atoms cause additional splittings, shown enlarged for the $F_1=1$ component at the right-hand side of the figure. The strong (weak) $F_1' \rightarrow F_1''$ transitions observed in the experimental spectra are indicated by solid (dashed) arrows.

standard deviations larger than the actual value of the parameters are obtained when attempting to fit these parameters.

In Fig. 5 the energy-level structure of ¹⁴ND₃ ($|J,K\rangle=|1,1\rangle$), as obtained from the best fit to the experimental data, is shown. Zero energy is chosen as the position of the lower inversion doublet component when all interactions are switched off, i.e., when all parameters in the first column of Table I except c_t are equal to zero. The main splitting in three sets of levels, labeled by the quantum number F_1 , in each of the components of the inversion doublet is caused by the quadrupole interaction of the ¹⁴N nucleus, as discussed before. The nuclear spins of the deuterium atoms cause additional splittings, shown enlarged for the $F_1=1$ component on the right-hand side of the figure. Within each component of the inversion doublet, all hyperfine levels are within an approximate 1.5 MHz energy range. In the figure, the (groups of) transitions observed in the spectra shown in Fig. 2 are schematically indicated. The energies of the 32 hyperfine levels (16 levels for each component of the inversion doublet) are given in Table II, together with the quantum numbers F_1 , I_D , and F .

With all the hyperfine levels of the $|J,K\rangle=|1,1\rangle$ state in ¹⁴ND₃ known, the splitting and shifting of the individual hyperfine levels in external electric fields can be calculated, using the same tensor coupling scheme. For this, the block matrices describing the levels in the s -symmetry and the a -symmetry components are coupled via the appropriate $\vec{E} \cdot \vec{d}$ coupling terms, and the full matrix is diagonalized. In Fig. 6 the calculated Stark shift for the manifold of hyperfine levels is shown in electric fields up to 100 V/cm. It is seen from this figure that none of the M_F components of the two $F_1=0$ hyperfine levels in the a -symmetry component of the inversion doublet is low-field seeking. Molecules in these two levels will not be focused therefore, explaining the absence of the transitions originating from these levels in spectra that are recorded when the hexapole is operated with constant voltages, as discussed earlier. Only the $F=4$ level

TABLE II. Hyperfine energy levels for $^{14}\text{ND}_3$ ($|J,K\rangle=|1,1\rangle$) as obtained from the best fit to the experimental data. For each hyperfine level, the number of M_F components that is shifted (up in the a -symmetry level or down in the s -symmetry level) is indicated.

s level					a level				
F_1	I_D	F	Energy (MHz)	Levels shifted	F_1	I_D	F	Energy (MHz)	Levels shifted
0	2	2	-1.0322	All	0	1	1	1587.9758	0
0	1	1	-1.0312	All	0	2	2	1587.9758	0
2	2	3	-0.1506	All	2	2	0	1588.8262	0
2	1	1	-0.1431	All	2	2	1	1588.8532	0
2	2	2	-0.1138	All	2	1	2	1588.8566	0
2	1	3	-0.1107	All	2	2	4	1588.8839	2
2	2	4	-0.0780	All	2	1	3	1588.9069	All
2	2	1	-0.0625	All	2	2	2	1588.9387	All
2	1	2	-0.0576	All	2	1	1	1588.9651	All
2	2	0	-0.0118	All	2	2	3	1588.9665	All
1	2	1	0.4684	0	1	1	0	1589.4678	All
1	1	1	0.4938	0	1	2	2	1589.4819	All
1	2	3	0.4976	0	1	1	2	1589.5150	All
1	1	2	0.5141	0	1	2	3	1589.5301	All
1	2	2	0.5526	0	1	1	1	1589.5302	All
1	1	0	0.5680	0	1	2	1	1589.5968	All

of the central group of $F_1=2$ hyperfine levels in the upper component of the inversion doublet has both M_F components that are low-field seeking, and M_F components that are hardly shifted in energy in an electric field. The most interesting, and *a priori* not expected, feature of the Stark curves shown in Fig. 6 is that four hyperfine levels of the $F_1=2$ group of levels, as well as all hyperfine levels belonging to

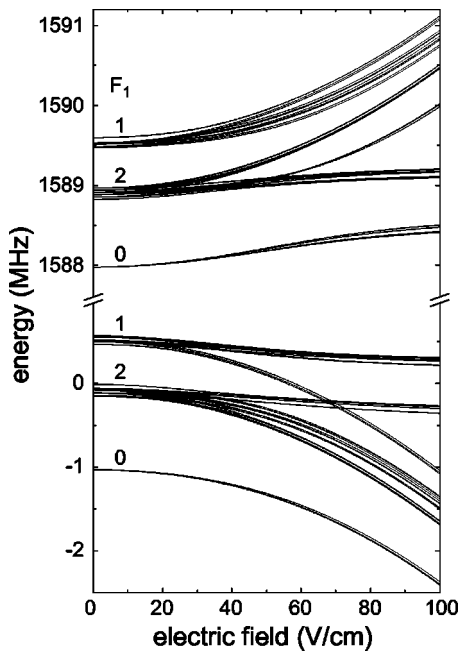


FIG. 6. Calculated Stark shift for the manifold of hyperfine levels of $^{14}\text{ND}_3$ in electric fields up to 100 V/cm.

the highest energy $F_1=1$ group of levels in the upper component of the inversion doublet are exclusively low-field seeking. For each hyperfine level the number of M_F components that is shifted in an electric field (up for the a -symmetry component and down for the s -symmetry component) is summarized in Table II.

When different M_F components are degenerate in zero electric field, Majorana transitions can occur. In the Stark decelerator, for instance, the molecules pass through an array of electric-field sections that are switched a large number of times from high field to low field. In that case, “low fields” are typically still a few kV/cm, i.e., (very) far from zero electric field, preventing Majorana transitions that would otherwise lead to beam loss. The rapid switching of the field in the decelerator will lead to scrambling between the various low-field seeking M_F components, as these stay within a few megahertz from each other almost independent of the strength of the electric field, but this does not lead to beam loss. In the quadrupolar electrostatic trapping geometry that we have used thus far for trapping of the ND_3 molecules, however, the electric field is really zero at the trap center [13]. Here, the trapped ammonia molecules, i.e., the ammonia molecules in low-field seeking M_F levels, can undergo Majorana transitions, possibly leading to trap loss. As, preferentially, the coldest molecules are removed via those Majorana transitions, this leads to heating of the remaining sample of trapped molecules in thermalizing collisions as well. Majorana transitions can be avoided in an electrostatic trapping geometry with a nonzero electric field at the trapping center, and design studies for such a trap, the analog of the Ioffe-Pritchard magnetic trap, have been made [38].

For those hyperfine levels of ammonia that are exclusively low-field seeking, trap loss due to Majorana transitions can simply not occur, enabling to stably confine these molecules in a trapping geometry with a true zero-electric-field region inside. This property is highly relevant and can, for instance, be exploited in future high-resolution spectroscopy studies. In the quadrupole electrostatic trap, the trapped $^{14}\text{ND}_3$ molecules are initially equally distributed over the various low-field seeking M_F states. Even if Majorana transitions are efficient, only molecules in the low-field seeking M_F components of the $F_1=2$, $F=4$ hyperfine level (two out of 48 populated M_F components) can be lost from the trap in the absence of collisions.

C. Energy levels, fitting parameters, and Stark effect for $^{15}\text{ND}_3$

The high-resolution inversion spectrum has been recorded for the $|J,K\rangle=|1,1\rangle$ level in $^{15}\text{ND}_3$ as well, and the full spectrum is shown in Fig. 7. As the ^{15}N nucleus has no quadrupole moment, the main splitting pattern that could immediately be recognized in the spectrum of $^{14}\text{ND}_3$ is now absent, and the whole spectrum covers less than 400 kHz. The upper part shows the spectrum obtained when the hexapole is operated in the pulsed mode, together with the simulated spectrum. The lower part shows the spectrum obtained when a constant voltage is applied to the hexapole. Clearly, several lines are absent and relative line intensities of other

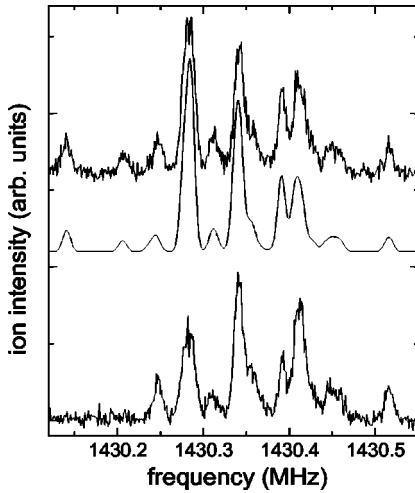


FIG. 7. High-resolution pure inversion spectra of $^{15}\text{ND}_3$ ($|J,K\rangle=|1,1\rangle$), measured by probing the lower inversion level. The upper experimental spectrum is recorded while operating the hexapole in the pulsed mode, and is shown together with the theoretical spectrum obtained from the best fit to the experimental data. The lower experimental spectrum is recorded when the molecules leave the hexapole adiabatically.

lines are different compared to the upper spectrum. From the good match of the simulated spectrum to the upper experimental spectrum, it can be concluded that the redistribution amongst the various hyperfine levels of the upper component of the inversion doublet is nearly complete when the voltages on the hexapole are rapidly switched on and off.

The parameters in the Hamiltonian that are obtained from a fit to the transition frequencies of 13 more or less isolated lines in the spectrum of $^{15}\text{ND}_3$ are listed in the last column of Table I. An approximate initial value for these parameters is now obtained by scaling the parameters found for $^{14}\text{ND}_3$. The energies of the 22 hyperfine levels (11 levels for each component of the inversion doublet) are given in Table III, together with the quantum numbers F_1 , I_D , and F , and the number of M_F components that is shifted when an electric field is applied.

In Fig. 8 the calculated Stark shift for the manifold of hyperfine levels of $^{15}\text{ND}_3$ is shown in electric fields up to 100 V/cm. It is seen that also in this case seven out of 11 hyperfine levels in the upper component of the inversion doublet are exclusively low-field seeking, and no Majorana transitions are possible for these levels. As the hyperfine levels in each component of the inversion doublet are within 300 kHz from each other, it is clear that the redistribution of the population over the various hyperfine levels by rapidly switching the fields in the hexapole is rather efficient.

IV. CONCLUSIONS

In a molecular-beam microwave-UV double-resonance spectrometer high-resolution pure inversion spectra have been obtained for $^{14}\text{ND}_3$ and $^{15}\text{ND}_3$ para-ammonia molecules in their ground state. A detailed analysis of the spectra has provided the hyperfine energy levels with their quantum number assignment for both these ammonia isotomers,

TABLE III. Hyperfine energy levels for $^{15}\text{ND}_3$ ($|J,K\rangle=|1,1\rangle$) as obtained from the best fit to the experimental data. For each hyperfine level, the number of M_F components that is shifted (up in the a -symmetry level or down in the s -symmetry level) is indicated.

s level					a level				
F_1	I_D	F	Energy (MHz)	Levels shifted	F_1	I_D	F	Energy (MHz)	Levels shifted
3/2	1	1/2	-0.1186	All	3/2	1	3/2	1430.1978	0
3/2	2	5/2	-0.0853	All	3/2	2	1/2	1430.1990	0
3/2	2	3/2	-0.0816	All	3/2	2	7/2	1430.3086	2
3/2	1	5/2	-0.0139	All	1/2	2	5/2	1430.3149	2
1/2	1	3/2	-0.0090	All	3/2	1	5/2	1430.3328	All
3/2	2	7/2	0.0196	All	3/2	1	3/2	1430.3362	All
1/2	2	5/2	0.0247	2	3/2	2	1/2	1430.3405	All
3/2	1	3/2	0.0519	0	1/2	1	3/2	1430.3462	All
1/2	1	1/2	0.0560	0	1/2	2	3/2	1430.4353	All
3/2	2	1/2	0.0926	0	3/2	2	5/2	1430.4366	All
1/2	2	3/2	0.0966	0	3/2	1	1/2	1430.4627	All

thereby completing the dataset for the symmetric top ammonia isotomers, as shown in Table I. The behavior of the manifold of hyperfine levels in external electric fields is calculated, and its implications for molecular-beam deceleration and electrostatic trapping experiments are discussed. In particular, it is noted that most hyperfine levels in deuterated ammonia are exclusively low-field seeking. Molecules in these hyperfine levels can be trapped in regions with a true zero electric field, as potential experimental loss processes due to Majorana transitions are avoided. It is difficult to more generally predict if a certain molecule will have this property in electric fields. A necessary requirement for this is that the quadratic Stark effect dominates over the linear Stark effect and that at least one of the atoms in the molecule has

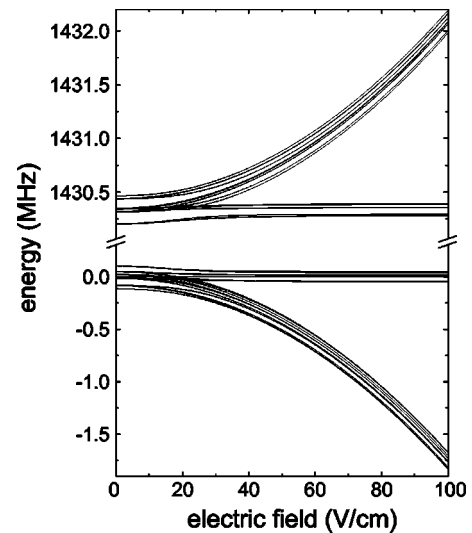


FIG. 8. Calculated Stark shift for the manifold of hyperfine levels of $^{15}\text{ND}_3$ in electric fields up to 100 V/cm.

a nuclear spin. All symmetric top ammonia isotopomers share this property.

In the present experiments, we have rapidly switched the electric field in the hexapole on and off to achieve a near complete redistribution of the ammonia molecules over the various hyperfine levels prior to entering the rf-interaction region. This was mainly done to have better defined initial conditions in the microwave experiment, to simplify the interpretation of the experimental data, and to get additional spectroscopic information. By implementing a separate electric-field section with time-varying homogeneous electric fields in between the hexapole and the rf-interaction region, transitions between hyperfine levels can be induced in a more controlled way. From the calculated Stark curves it can be deduced which field strengths and switching times are required to optimize or minimize the population redistribution. It is expected that in this case the redistribution of the molecules over the various hyperfine levels can be quantitatively understood and controlled. Preparation of a beam of ammonia molecules in selected (subsets of) hyperfine levels, either via controlled redistribution or via rf transitions, will be important for future scattering and trapping experiments.

In future molecular-beam experiments, the resolution in the microwave spectra can still be significantly improved by lengthening the interaction time of the molecules with the rf radiation. This can be achieved by enlarging the rf-interaction region and/or by reducing the average velocity of the molecular beam, e.g., by passing the molecular beam through a Stark decelerator or through an alternate gradient decelerator prior to entering the rf interaction region [10–12]. Ultimately, these rf-transitions are measured for the ammonia molecules stored in the trap, in which case the spectral resolution is only limited by the trapping time.

ACKNOWLEDGMENTS

This work is part of the research program of the “Stichting voor Fundamenteel Onderzoek der Materie (FOM),” which is financially supported by the “Nederlandse Organisatie voor Wetenschappelijk Onderzoek (NWO).” The research of R.T.J. has been made possible by a fellowship of the Royal Netherlands Academy of Arts and Sciences. We thank André J. A. van Roij and Paul H. M. Smeets for expert technical support and H. L. Bethlem for useful discussions.

-
- [1] J. M. Doyle and B. Friedrich, *Nature (London)* **401**, 749 (1999).
- [2] C. J. Williams and P. S. Julienne, *Science* **287**, 986 (2000).
- [3] M. Baranov, L. Dobrek, K. Góral, L. Santos, and M. Lewenstein, e-print cond-mat/0201100.
- [4] L. Santos, G. V. Shlyapnikov, P. Zoller, and M. Lewenstein, *Phys. Rev. Lett.* **85**, 1791 (2000).
- [5] M. A. Baranov, M. S. Mar’enko, Val. S. Rychkov, and G. V. Shlyapnikov, *Phys. Rev. A* **66**, 013606 (2002).
- [6] D. DeMille, *Phys. Rev. Lett.* **88**, 067901 (2002).
- [7] T. Takekoshi, B. M. Patterson, and R. J. Knize, *Phys. Rev. Lett.* **81**, 5105 (1998).
- [8] N. Vanhaecke, W. de Souza Melo, B. L. Tolra, D. Comparat, and P. Pillet, *Phys. Rev. Lett.* **89**, 063001 (2002).
- [9] J. D. Weinstein, R. deCarvalho, T. Guillet, B. Friedrich, and J. M. Doyle, *Nature (London)* **395**, 148 (1998).
- [10] H. L. Bethlem, G. Berden, and G. Meijer, *Phys. Rev. Lett.* **83**, 1558 (1999).
- [11] H. L. Bethlem, G. Berden, A. J. A. van Roij, F. M. H. Crompvoets, and G. Meijer, *Phys. Rev. Lett.* **84**, 5744 (2000).
- [12] H. L. Bethlem, A. J. A. van Roij, R. T. Jongma, and G. Meijer, *Phys. Rev. Lett.* **88**, 133003 (2002).
- [13] H. L. Bethlem, G. Berden, F. M. H. Crompvoets, R. T. Jongma, A. J. A. van Roij, and G. Meijer, *Nature (London)* **406**, 491 (2000).
- [14] F. M. H. Crompvoets, H. L. Bethlem, R. T. Jongma, and G. Meijer, *Nature (London)* **411**, 174 (2001).
- [15] H. L. Bethlem, F. M. H. Crompvoets, R. T. Jongma, S. Y. T. van de Meerakker, and G. Meijer, *Phys. Rev. A* **65**, 053416 (2002).
- [16] W. Ketterle and N. J. van Druten, *Adv. At., Mol., Opt. Phys.* **37**, 181 (1996).
- [17] G. R. Gunther-Mohr, R. L. White, A. L. Schawlow, W. E. Good, and D. K. Coles, *Phys. Rev.* **94**, 1184 (1954).
- [18] G. R. Gunther-Mohr, C. H. Townes, and J. H. van Vleck, *Phys. Rev.* **94**, 1191 (1954).
- [19] J. P. Gordon, *Phys. Rev.* **99**, 1253 (1955).
- [20] J. P. Gordon, H. J. Zieger, and C. H. Townes, *Phys. Rev.* **99**, 1264 (1955).
- [21] G. F. Hadley, *J. Chem. Phys.* **26**, 1482 (1957).
- [22] G. F. Hadley, *Phys. Rev.* **108**, 291 (1957).
- [23] K. Shimoda and K. Kondo, *J. Phys. Soc. Jpn.* **15**, 1125 (1960).
- [24] K. Kondo and K. Shimoda, *J. Phys. Soc. Jpn.* **20**, 437 (1965).
- [25] S. G. Kukulich, *Phys. Rev.* **156**, 83 (1967); note that the power of the phase factor in the last formula of this paper should read $J + I_N + 2F'_1 + F + I$, as also remarked by Ch. Chardonnet (private communication).
- [26] R. G. Nuckolls, L. J. Rueger, and H. Lyons, *Phys. Rev.* **89**, 1101 (1953).
- [27] G. Hermann, *J. Chem. Phys.* **29**, 875 (1958).
- [28] S. N. Murzin and B. D. Osipov, *Opt. Spektrosk.* **52**, 242 (1982).
- [29] S. N. Murzin and B. D. Osipov, *Opt. Spektrosk.* **53**, 579 (1983).
- [30] S. N. Murzin, *Opt. Spektrosk.* **59**, 438 (1995).
- [31] L. Fusina, M. Carlotti, and D. Di Lonardo, *J. Mol. Spectrosc.* **147**, 71 (1991).
- [32] L. Fusina and S. N. Murzin, *J. Mol. Spectrosc.* **167**, 464 (1994).
- [33] H. Howe, Jr., *Stripline Circuit Design* (Artech House, Inc., Norwood, MA, 1974).
- [34] M. N. R. Ashfold, R. N. Dixon, N. Little, R. J. Stickland, and C. M. Western, *J. Chem. Phys.* **89**, 1754 (1988).
- [35] B. Sartakov *et al.* (unpublished).

- [36] L. D. Landau and E. M. Lifshitz, *Quantum Mechanics, Non-Relativistic Theory*, 3rd ed. (translated from Russian by J. B. Sykes and J. S. Bell) (Pergamon Press, Oxford, 1977).
- [37] In Ref. [25] every time that $g_{H,N}$ appears it should be replaced by $g_{H,N}/I_{H,N}$. This leads to a $2^{1/3}$ larger N–H bond length than determined in Ref. [25], in good agreement with literature values.
- [38] G. Xu, Ph.D. thesis, The University of Texas, Austin, 2001 (unpublished).